PCCP

Transition from Covalent to Noncovalent Bonding between Tetrel Atoms

Journal:	*Physical Chemistry Chemical Physics*
Manuscript ID	CP-ART-04-2024-001598.R1
Article Type:	Paper
Date Submitted by the Author:	14-May-2024
Complete List of Authors:	Scheiner, Steve; Utah State University, Department of Chemistry and Biochemistry

Transition from Covalent to Noncovalent Bonding between Tetrel Atoms

Steve Scheiner*

[a]Department of Chemistry and Biochemistry
Utah State University
Logan, Utah 84322-0300
USA

*email: steve.scheiner@usu.edu

Abstract

The strength and nature of the bonding between tetrel (T) atoms in $R_2T\cdot\cdot TR_2$ is examined by quantum calculations. T atoms cover the range of Group 14 atoms from C to Pb, and substituents R include Cl, F, and NH_2. Systems vary from electrically neutral to both positive and negative overall charged radicals. There is a steady weakening progression in T-T bond strength as the tetrel atom grows larger, transitioning smoothly from a strong covalent to a much weaker noncovalent bond for the larger T atoms. The latter have some of the characteristics of a ditetrel bond, but there are also significant deviations from a classic bond of this type. The $T_2Cl_4^-$ anions are more strongly bonded than the corresponding cations, which are in turn stronger than the neutrals.

Keywords: AIM; SAPT; Tetrel Bond

INTRODUCTION

The classic single and double CC bonds of molecules like ethane and ethylene constitute one of the foundations of organic chemistry. Some of their defining characteristics are the nearly free rotation around the single C-C bond, and inhibited rotation around the stronger C=C bond that holds molecules in either a cis or trans planar geometry. Less studied are the ways in which these bonds are modified by the replacement of C with some of its heavier Group 14 tetrel atom counterparts in these sorts of bonding situations. Some of the heavier-atom analogues of ethane, ethylene, acetylene, and benzene have been isolated and examined over the years [1-4]. For example, the Si=Si bondlength in RClSi=SiClR has been measured to be 2.553 Å, longer than 2.108 Å in its triple-bonded RSi≡SiR congener [5]. Skipping down a row in the periodic table to RGe≡GeR leads to a comparable bond length of some 2.21-2.25 Å, while that in the heavier $Ph_3Pb{\equiv}PbPh_3$ is 2.848 Å. But these geometries differ from their C analogues in some important respects. They generally take on a characteristic trans-bent structure, as opposed to the planar ethylene derivatives. Such a geometry was noted [5] in a recent digermylene dianion with an especially long Ge-Ge bondlength of 2.877 Å, as compared to several others in this class [6-8].

As a particularly interesting new insight into this field, a very recent study [9] found that two Sn atoms can form an unexpectedly stable bond with one another in the context of a radical anion, which was confirmed by a combination of crystal structure analysis, EPR spectroscopy, and reactivity. Each Sn atom was liganded to a pair of N atoms within a five-membered ring of a o-phenylenediamido ligand. The relatively short Sn··Sn distance of 3.215 Å, coupled with DFT computations, led the authors to characterize this interaction as a 1-e/2-c bond. This finding represents the first report of such a bond between Sn atoms, and indeed between any of the tetrel series.

These results raise a number of interesting fundamental questions about chemical bonding, which are addressed here by extensive quantum chemical calculations. In the first place, is there something unique about the ditopic o-phenylenediamido ligand which leads to this sort of bonding, or is this phenomenon a more general one that would occur for other, monotopic ligands? On a related matter, is Sn the only tetrel atom which can bond in this manner, or is it a general feature of all the tetrel atoms? If so, it would be instructive to determine how the bonding alters along the Group 14 list of atoms. How might the bonding pattern change if the species is positively, instead of negatively charged, or is electrically neutral for that matter? What is the effect on the binding of alteration of ligand, considering both electron-withdrawing and donating.

These issues are examined here by high-level quantum chemical calculations in the context of a wide range of $(R_2T{\cdot\cdot}TR_2)^x$ species. The overall charge x is taken as +1 and 0 as well as -1. The R ligands vary from electron-withdrawing Cl and F, to the donating NH_2 group. The entire list of T atoms, from C down to Pb are considered as well. This study can therefore address as to whether the transition from the weak Sn··Sn interaction observed in the original anion, to the much stronger and shorter C=C bonds in the C-analogues is a gradual strengthening process, or changes in large steps.

METHODS

Quantum chemical calculations were performed via the density functional theory (DFT) approach, within the context of the M06-2X functional [10] and a polarized triple-ζ def2-TZVP basis set. This combination has been assessed as highly accurate for interactions of the sort examined here [11-18]. The Gaussian 16 [19] program was chosen as the specific means to conduct these computations. Atoms in Molecules (AIM) bond paths and their associated critical points [20] were located and their properties evaluated by AIMAll [21]. The Wiberg Bond Index was measured with the aid of the NBO package contained within Gaussian. All interaction energies were corrected for basis set superposition error through the Boys-Bernardi counterpoise protocol [22]. Total interaction energies were decomposed into their contributing constituents by Symmetry-Adapted Perturbation Theory (SAPT) [23, 24] at the SAPT0 level through the PSI4 program [25] in the context of the same def2-TZVP basis set.

RESULTS

Geometries

The geometries of the anionic $T_2Cl_4^-$ species are illustrated in Fig 1a. In line with the growing size of the T atom, the T-T distance elongates as one moves down the tetrel column of the periodic table. There is a good deal of variation, from 1.432 Å for C up to 3.235 Å for Pb. There are some variations in other facets of the geometry as well. The anions take on a sort of stacked shape, where the two TCl_2 units are roughly parallel to one another, with the Cl atoms pointing in opposite directions. The angles between each of these two planes and the T-T axis reported in the first column of Table 1 are all larger than 90°, particularly so for $C_2Cl_4^-$ where the planes make an angle of 135° with T-T. The $Pb_2Cl_4^-$ geometry is interesting in that the two $PbCl_2$ planes are skewed with respect to one another. One measure of this skewing is the very different θ(PbPbCl) angles to the two Cl atoms of each unit, which are 73° and 108°.

The geometries of the $T_2Cl_4^+$ cations in Fig 1b are different in certain respects. In the first place, the R(TT) bondlengths are somewhat shorter with the exception of T=Pb. There are fundamental differences in shape from one T to the next. $C_2Cl_4^+$ is fully planar, but the Si and Ge atoms are puckered. The angle made by each TCl_2 plane with the T-T axis is 149° and 141° for Si and Ge, respectively, as delineated in Table 1. The geometry changes once again for the two heavier T atoms. Rather than the symmetric structures of the preceding cations, a strong asymmetry is introduced wherein the planes of the two TCl_2 units are nearly perpendicular. One plane makes an angle of 110° with the T-T axis, while the other angle is much larger, between 166° and 174°.

With regard to neutral systems, neither Sn nor Pb form a stable T_2Cl_4 molecule. C_2Cl_4 is of course fully planar, as indicated in Fig 2, while the geometries of the Si and Ge counterparts are in a sense intermediate between their corresponding cations and anions. Specifically, the angles between the planes in Table 1 are larger than in the anion, but smaller than the cation.

The T-T distances unsurprisingly increase as the size of the T atom grows from left to right in Figs 1 and 2. In order to view these bondlengths on a more even footing, a reduced bondlength R_{red} was evaluated as the ratio between this distance and the T-T bondlength in the neutral hydrogenated $H_3T\text{-}TH_3$ that contains a clear single bond. (These latter bondlengths are 1.524, 2.335, 2.447, 2.805,, and 2.861 Å for C through Pb.) These reduced bondlengths are displayed in Fig 3 where several patterns are clearly in evidence. In the first place, even after being reduced by comparison to a single bondlength, R_{red} still grows from left to right as T becomes larger, suggesting a progressive bond weakening. Secondly, for the lighter T atoms, the bond is shorter for the anion than for the cation, but this pattern reverses for Pb. As for the neutral system, this bond is quite short for Cl_2CCCl_2, but grows quickly as T is enlarged, so represents the longest bond for $Cl_2GeGeCl_2$.

It is also interesting to compare these bonds to the classic single bond in $H_3T\text{-}TH_3$. Some of the systems on the left side of Fig 3 have a reduced R of less than unity, suggesting a certain amount of double bond character. Such is unsurprising for the ethylenic neutral Cl_2CCCl_2, but seems to extend to the cation and anion as well, albeit not quite as short. This double bond character diminishes quickly as T grows larger and R_{red} becomes greater than 1, nearly 1.2 for $Pb_2Cl_4^-$.

Energetics

An energetic measure of the strength of each T-T bond emerges from the energy of the dissociation energy ΔE of the reaction

$$T_2Cl_4^x \rightarrow TCl_2 + TCl_2^x \quad (1)$$

where x represents the charge, either -1, 0, or +1. It is first apparent from Table 2 that all of these bonds, from classic single to those in $T_2Cl_4^x$ weaken quickly as T grows larger. The single bond in T_2H_6 is weakened upon chlorination. In elucidating the effect of the charge on the T-T bond in $T_2Cl_4^x$, the anion contains the strongest bond for the heavier T, but the reverse is true for C. Indeed the T=C cases are unique in that it is only here for which the $C_2Cl_4^x$ bonds are stronger than C_2H_6 or C_2Cl_6. The loss of charge severely weakens the T_2Cl_4 bond, to the point where it disappears entirely for Sn and Pb. However, the same is not true for C_2Cl_4 where the neutral contains the strongest C-C bond. To be sure that the results are not biased by a particular choice of basis set, the dissociation energies of the various anions were recomputed with the much larger and more flexible quadruple-ζ def2-QZVPP basis set. The results are presented in parentheses in Table 2 where it may be seen that there is little variation from the smaller set data.

Many of the energetic trends in Table 2 and visualized in Fig 4 are mirrored in the reduced bondlengths in Fig 3. The reduction in T-T bond strength with larger T evident in Fig 4 is reproduced by rising patterns of all three curves in Fig 3, and most particularly of the rapid increase within the black curve for the neutrals. The shorter T-T bonds within the anion are reflected by larger bond energies. However, there are differences as well. For example, the much stronger Pb-Pb within the anion contrasts with its longer bondlength.

There is a sentiment in the literature that the density of the AIM bond critical point ought to serve as a valid metric as to bond strength. This quantity is listed in Table 3 for the various T_2Cl_4 systems, again along with those for T_2H_6 and T_2Cl_6 as points of reference. These values of ρ are all larger than 0.5 au for the latter single bonds, with little distinction as to whether H or Cl substituent. And the density pattern is consistent with a weakening of the bond with larger T. The effects of the identity of T or the charge on the T_2Cl_4 may be best seen when compared with these classic single bonds as a reduced ρ, again taking T_2H_6 as reference. These ρ_{red} in Fig 5 are larger than unity for T=C, consistent with the ethylenic character, particularly for the neutral. But this reduced density drops quickly as T is enlarged, suggesting the bonds are weaker than a single T-T bond, with ρ_{red} less than 0.5 for Pb.

There is no clear consensus regarding the value of ρ that serves as a threshold between a covalent and noncovalent bond. But if one were to reasonably take 0.4 as such a threshold, then the Sn··Sn and Pb··Pb interactions might be taken as noncovalent ditetrel bonds, perhaps also the Ge··Ge bond in neutral Ge_2Cl_4. All of the latter systems are consistent in that they contain a density below 0.4.

Another measure of the strength of the T-T bond arises in the context of the Wiberg bond index (WBI), listed in the right side of Table 3. The values for the neutral T_2H_6 and T_2Cl_6 are near unity for C, but diminish for the heavier T atoms, particularly the chlorosubstituted molecules, for which WBI drops down to 0.6 for Pb_2Cl_6. Although WBI exceeds unity for the three C_2Cl_4 species, it too drops quickly for larger T. These quantities are rather small for the Pb moieties, especially $Pb_2H_4^+$ where it is 0.23. Like the BCP densities, WBI is larger for the T_2Cl_4 cation than for the anion when T is Si or Ge, but this pattern reverses for Sn and Pb. Also in common with ρ_{BCP}, the bond apparently fades from covalent to noncovalent for the larger T atoms.

With respect to distinguishing noncovalent from covalent, there are ideas expressed in the literature concerning other facets of the AIM analysis of density topology. It is commonly taken that the sign of the total energy density H can be used to mark this distinction. All values of H in Table 4 are negative, suggesting at least some degree of covalency. On the other hand, these quantities are quite small in magnitude toward the bottom of the table, clouding such an interpretation. For all T larger than C, H is considerably less negative for T_2Cl_4 than for the single bonds of T_2H_6 and T_2Cl_6 so are correspondingly less covalent. The sign of the density Laplacian is taken as another indicator, with covalency signaled by a negative value. The $\nabla^2\rho$ entries in Table 4 are clearly very negative for the smaller T atoms, but quickly diminish in magnitude, and switch sign for the larger T atoms. This particular indicator supports the idea that the larger T_2Cl_4 systems are held together by noncovalent ditetrel bonds. Indeed, one could make the case through $\nabla^2\rho$ of noncovalent bonding in both Pb_2H_6 and Pb_2Cl_6 as well.

One aspect of tetrel and related bonds derives from NBO analysis that identifies a certain amount of charge transfer from the electron donor unit, usually a lone pair, to a σ* antibonding orbital of the Lewis acid unit. For the majority of systems examined here, the bonding between Sn atoms is strong enough that NBO characterizes the complex as a single system, so this sort of

transfer does not occur. However, for some of the more weakly bound systems, NBO does indeed identify two separate entities, so such an analysis is possible. In the $Pb_2Cl_4^-$ anion, for example, there is a charge transfer from one Pb lone pair to a σ*(PbCl) orbital that amounts to 0.60 kcal/mol in terms of second order perturbation energy E2. This quantity is a bit larger at 0.92 kcal/mol for the corresponding cation. For the lighter $Sn_2Cl_4^-$, E2 is reduced to only 0.12 kcal/mol, while the cation's internal bond is strong enough that NBO characterizes it as a single unit. So from a NBO perspective, it is only $Pb_2Cl_4^-$, $Pb_2Cl_4^+$, and $Sn_2Cl_4^-$ that would be thought of as containing some elements of a noncovalent ditetrel bond. NBO is thus in rough agreement with the ρ_{BCP} cutoff of 0.4 for ρ_{BCP}, or a 0.5 threshold of WBI for distinguishing a covalent from a noncovalent bond. There is also consistency that the same distinction can be made on the basis of the sign of $\nabla^2\rho$.

Factors Contributing to Shape

As indicated above, the cationic and anionic systems assume somewhat different shapes. With some exceptions, the anions are generally stacked with TCl_2 planes roughly parallel, with more variation in the cations. Some rationale for these shapes is derived from analysis of the frontier MOs of the two TCl_2 units. The upper half of Fig 6 displays the distributions of the HOMO of the anionic TCl_2^- and the LUMO of the neutral with which it would interact. The strong overlap between the green segments helps account for the stacked geometry of these anions, both for Si on the left and for Sn on the right.

The cationic systems can be characterized by the interaction between the HOMO of the neutral TCl_2 and the LUMO of the TCl_2^+. The diagrams of these respective MOs in the lower half of Fig 6 help explain the different shapes of the Si and Sn cations. These two orbitals best overlap when the two Si atoms are nearly pointing toward one another, whereas the situation changes for Sn. In this case, the LUMO of $SnCl_2^+$ best aligns with the HOMO of $SnCl_2$ when the two units are in a more perpendicular geometry. It should be noted as well that the energy differences between the various HOMO-LUMO pairs are fairly small, assisting in their mutual interaction.

Particularly when dealing with noncovalent interactions, it has been found useful to consider how the molecular electrostatic potentials (MEPs) of the two constituent monomers might best align with one another [26-33]. The MEPs of the three charge states of $SnCl_2$ are illustrated in Fig 7. The MEP surrounding the anion is of course negative throughout, while it is positive for the cation. The extremes of each have been adjusted so as to best illustrate the variation over space. So for the anion, the blue color indicates the least negative region, while the red color for the cation shows where the MEP is least positive. Of course, for all three charge states, the Cl atoms are surrounded by red, with blue areas around the Sn.

Given the geometries of the various dimers, of most interest is the disposition of MEP around the central Sn. Fig 7a presents the alignment of the MEP of the neutral in the lower half and that of the anion above, with the two molecules placed in the parallel stacked arrangement of the $Sn_2Cl_4^-$ system. The blue π-hole of the neutral contacts the green region of the upper anion, less

negative than the Cl atoms, but avoiding the blue σ-hole of the Sn, which is much less negative. A similar diagram in Fig 7b displays a similar diagram for the geometry of the $Sn_2Cl_4^+$ cation. In this case, there is a higher degree of contact between blue areas of the two units, so the simple Coulombic interaction is not as favorable.

Overall, the interactions of these two ionic systems are not heavily guided by electrostatic considerations, which would of their own accord favor interactions between the Sn atom of one unit and Cl atoms of its partner. On the other hand, one can see a tendency of the bluest and most positive regions to avoid one another to at least a limited extent.

Other Systems

Rather than focus purely on the chlorinated systems, it is worthwhile to examine how the properties are influenced by other substituents. F can be taken as an example of a more electron-withdrawing substituent while NH_2 is an electron-donating unit. The geometries and other aspects of the systems containing various combinations of these substituents for the T=Sn units are displayed in Fig 8, along with Sn_2Cl_4 for ease of comparison. The anions are contained in Fig 8a at the top and cations in the bottom Fig 8b. Each large black number refers to ΔE, the dissociation energy, while bond critical point densities are displayed as red numbers.

It should be noted first that the overall shapes of these complexes are much like those for the chlorinated systems on the far left, stacked parallel anions and T-shaped cations. The switch from Cl to F has only a very minor influence on the energetics, while causing a small lengthening of R(Sn-Sn), coupled to a small decrease in ρ_{BCP}. A much larger perturbation occurs when NH_2 groups are added. The anion is weakened from 39.0 to 25.8 kcal/mol, while the cation is significantly strengthened. These changes are accompanied by the corresponding changes in both the Sn-Sn bondlength and density.

It is also of interest to consider a mixed dimer, pairing SnF_2 with $Sn(NH_2)_2$. The anion and cation forms are depicted on the right side of Figs 8a and 8b, respectively. The general shapes are quite similar to the homodimers on the left, and there are also minor adjustments in the Sn··Sn separation. The red BCP densities suggest the anion might be thought to have a good deal of noncovalent character while the cation is probably best described as covalent.

The dissociation energies depend upon which of the two subunits is considered as containing the charge before the complex is formed. Since F is more electronegative than NH_2, it is better able to contain a negative charge in SnF_2^-, so the $Sn(NH_2)_2/SnF_2^-$ set of monomers is more stable than $Sn(NH_2)_2^-/SnF_2$. Thus the dissociation energy with respect to the former pair is much less endothermic than when referenced to the latter. The converse is true for the cation as NH_2 can better contain a positive charge. The dissociation energy of $(NH_2)_2Sn\text{-}SnF_2^+$ is thus much smaller when referenced to $(NH_2)_2Sn^+$ plus SnF_2. The discrepant values of these mixed systems, depending upon the definition of the constituent monomers, should serve as a caution in drawing conclusions based solely on dissociation or binding energy.

DISCUSSION

The tetrasubstituted ditetrel systems span a wide range of bond type and strength, that depend upon the nature of the tetrel atom, the substituents, and the overall charge. The C_2Cl_4 systems all have a strong C=C double bond. Both the neutral and cation are planar, while the anion is substantially puckered at both C atoms. This puckering grows in the larger T_2Cl_4 systems, and the anions acquire a stacked parallel structure. The cations of Sn and Pb are better described as a sort of T-shape in that the planes of the two TCl_2 units are roughly perpendicular.

While the C-C bond lengths in these C_2Cl_4 systems of any charge are all shorter than the standard single bond in ethane, the opposite is found for larger T atoms. The ratio of the T-T bondlength to that in H_3T-TH_3 is greater than 1, and becomes progressively larger as the T atom grows in size. This reduced bondlength is shorter for the anion than the cation for Si and Ge, but the opposite is found for Pb.

These geometrical indicators of weakening T-T bond are verified by the dissociation energy of the two TCl_2 unit to form T_2Cl_4. While this quantity is in the 90-120 kcal/mol range for C, it is much smaller for the other T atoms, and grows progressively smaller as T becomes larger, particularly for the cation which drops steeply. These energies diminish in the order anion > cation > neutral. Indeed, the small dissociation energy of the neutral Si_2Cl_4 and Ge_2Cl_4, less than 10 kcal/mol, vanishes entirely for Sn and Pb where there is no stable neutral T_2Cl_4. The anion though, has a dissociation energy of some 40 kcal/mol for T atoms larger than C, which is fairly stable from one T atom to the next.

The patterns observed for the BCP density largely mirror the bondlengths. While all of the C systems have a density considerably larger than the single bond in C_2H_6, this quantity drops quickly as T grows larger. This ratio to the prototype single bond diminishes down below 0.6 for Pb. Like the reduced bondlengths, the anion has a stronger bond for Si and Ge, but it is the cation that is the stronger for Pb. On the basis of these density ratios, the Sn-Sn bond order could be assessed as 0.6, while that between Pb atoms is 0.4-0.5. In absolute terms, the BCP density of the C-C bonds is 0.3 or larger, but diminishes rapidly with T size. ρ_{BCP} is less than 0.04 for Sn and less than 0.03 for Pb. Considering total energy density H as a marker, this quantity is negative for all systems, suggesting at least some covalent character, but becomes vanishingly small in magnitude for Sn and Pb ionic systems, and even for neutral Ge_2Cl_4. These same systems with very small negative H, also present a positive density Laplacian, suggestive of primarily noncovalent character.

When viewed in concert with the Wiberg Bond Index, the bond types observed here might be categorized as follows. There are clearly very strong covalent bonds in the C_2Cl_4 systems, regardless of charge. All of these bonds quickly lengthen and weaken as T grows larger, especially the neutral which disappears for T larger than Ge. The anion generally contains a stronger T-T bond, although this seems to reverse for Pb for which the cation is more strongly bound. For the larger T atoms, it would be fair to claim that the bond is noncovalent, or at least contains only a minor element of covalency.

Overall, then, these systems cover a spectrum of bond measures. On one end of the spectrum are the alkene-like C_2Cl_4 systems of any charge, with a double C=C bond. Following a mostly smooth transition to heavier T atoms, and progressively weakening T-T bonds, the Pb systems on the other end of the spectrum would best be categorized as much longer and weaker noncovalent Pb··Pb ditetrel bonds. This label is supported by the finding of charge transfer from the lone pair of one Pb atom to the σ*(PbCl) orbital of its partner, albeit the values of E2 are fairly small. But there are caveats here as well. Unlike the majority of tetrel bonds in the literature [34-52], the stability of these systems are predicated on an overall charge, whether positive or negative. Secondly, one sees a coulombic interaction more nuanced than the classical contact between a positive σ or π-hole on one unit and a negative region on the partner molecule.

In order to elaborate further on this last point, the interaction energies of the more weakly bound T_2Cl_4 ions with T=Sn and Pb were dissected into their constituent components via SAPT. The results in Table 5 display several interesting patterns. The two anions are held together in roughly equal measure by electrostatic and induction forces, with a smaller contribution from dispersion. The cations were considered in two different modes. Mode (1) places the charge on the upper unit in Fig 1b, while it is the lower unit on which the charge resides in mode (2). In either case, the cations differ from the anions in some ways, the most important of which is the reversal of the ES component from strongly attractive to weakly so in one case, and repulsive in the three others. This repulsion is consistent with MEP diagrams in Fig 7 that place blue areas in coincidence with one another. Also as compared to the anions, the induction and dispersion components are somewhat reduced. The combined result is a much weaker binding in the cations than in the anions.

While the pattern of a large attractive ES component in the anions is consistent with most tetrel and related noncovalent bonds, the repulsive coulombic interaction in the cations might argue against their classification as a tetrel bond, at least as a classical one. The repulsive ES term is especially notable in light of the charge on one of the two units that would in many cases lead to a strong charge-assisted interaction. Another perspective of the binding in the Pb cations has to do with their small interaction energies. Even though the dispersion contribution is fairly small, the total interaction would be repulsive in its absence, so in this sense they might be thought of as dispersion-bound. It should perhaps be emphasized that the total interaction energies in Table 5 refer to monomers in the geometries they adopt within the dimer, so differ in definition from the dissociation energies in Table 2 which take fully optimized monomer geometries as their reference.

The classification of any of these weak T··T interactions as a TB would also involve a significant deviation from the bulk of such bonds in the literature [39, 53-60]. Whereas classical TBs are strengthened as the T atom is taken from lower segments of the periodic table, the bonds here follow an opposite pattern. There is a clear progressive weakening of the interaction for larger T atoms: C > Si > Ge> Sn > Pb.

The open-shell character of the cationic and anionic systems leaves a single electron in the highest occupied SOMO, whose disposition in space offers certain insights into the nature of the

bonding. These orbitals are displayed in Fig 9 for the C and Sn variants of $T_2Cl_4^+$ and $T_2Cl_4^-$. The case of $C_2Cl_4^+$ can be understood largely as the removal of one electron from the C-C π-bonding MO, leaving this orbital essentially unchanged. There are geometrical changes in the corresponding anion, leaving only a small amount of density along the C-C axis. Shifting attention to the Sn_2Cl_4 systems, the SOMO places some density along the Sn-Sn axis, particularly in the anion which may help explain its stronger bonding than the cation. In summary, while the SOMO of $C_2Cl_4^+$ contains π-symmetry, the other systems are characterized by σ-bonding within this orbital.

Some of the calculated properties can be compared with the very recent experimental results offered by Chan et al [9]. Their system paired two Sn atoms, each of which was covalently bonded to two N atoms within a five-membered ring within the context of phenylenediamido ligands. The system as a whole was a radical anion, so is most directly comparable to the $\{Sn(NH_2)_2\}_2^-$ anion in Fig 8a. The computed Sn··Sn distance in the latter is 3.207 Å, rather similar to the 3.215 Å measured in the former larger system. Also very similar are the Sn-N bondlengths, both 2.12 Å. The authors had calculated the Wiberg bond index of their complex to be 0.57, which compares with 0.51 for the smaller model system. One significant difference lies in the calculated dissociation energy of 43.5 kcal/mol for the larger system, compared with 25.8 kcal/mol for the model system containing NH_2 ligands rather than the larger phenylenediamido.

With regard to the lighter Ge, Ma et al [5] had deduced the geometry of a digermylene system similar to that examined by Chan et al [9], wherein each Ge is attached to two N atoms within a ring, in an overall trans-bent structure. One difference, however, is the double negative charge on this species, which led in part to the long Ge··Ge distance of 2.877 Å, as compared to 2.670 Å calculated here for the $Ge_2Cl_4^-$ monoanion, also with a similar trans-bent structure. The Si atoms of all three charge states were computed here to be puckered to some degree. However, they can be made more planar if conjugated to Si=C double bonds within the context of a cumulenic C=Si=Si=C arrangement [61]. But even so, there is a good deal of twisting in terms of the C-Si-Si-C torsion angles.

In a more general sense, the results presented here are consistent with prior experimental findings [2, 3] in other respects. The trans-pyramidal shapes of the neutral T_2Cl_4 units match prior structural data for T=Si and Ge. The failure to locate a minimum corresponding to these neutral molecules for Sn and Pb also agrees with experimental findings that any such species are very unstable and easily dissociate into pairs of TR_2 units when placed in solution.

These purported ditetrel bonds can be compared with several examples in the literature. A survey of the CSD [40] had provided a list of some 219 examples of two T atoms approaching in such a way as to suggest a ditetrel bond, 44 of which involved Pb··Pb pairs. In an example of such a system, a molecule was synthesized in which Pb was bound to four other atoms, O, S, and two N atoms. They were arranged quite differently from tetrahedral, all substituents lying on one side, leaving the other side exposed. A noncovalent Pb··Pb ditetrel bond was formed between two such molecules, despite the absence of a σ-hole on the Pb center. The interaction energy was calculated to be 19 kcal/mol, but some of this must be attributed to secondary

interactions. Subtraction of the latter suggested a ditetrel bond energy of some 10 kcal/mol. With regard to the Pb··Pb interaction itself, its BCP density is 0.008 au, quite a bit smaller than the values for the T_2Cl_4 ions with T=Sn and Pb examined here. Note, however, that the ES portion of the interaction energy was attractive, unlike some of the systems described above.

In another set of systems, a strong asymmetry was introduced in that one T atom serves as the electron donor due to its attachment to an electron-releasing substituent such as Li, while the substituent on the electron-accepting T is a strong electron withdrawing agent such as F [52]. Dissociation energies were calculated to lie in the range between 3 and 9 kcal/mol for the whole spectrum of T atoms from C to Pb. The range in the T_2Cl_4 ions with T=Sn and Pb was much broader, from only 0.6 kcal/mol for $Pb_2Cl_4^+$ up to 39 kcal/mol for $Sn_2Cl_4^-$. The AIM bond critical point densities for the former systems were between 0.005 and 0.011 au, quite a bit smaller than the 0.021 - 0.038 au range for the T_2Cl_4 ions. The systems considered here are more symmetric in that it is a pair of identical TCl_2 units that are interacting with one another through their T centers. On the other hand, one can attribute strong electron donating properties to a TCl_2^- anion when paired with a neutral TCl_2, with a clear asymmetry between the two; likewise for TCl_2 and TCl_2^+ where the latter serves as an electron deficient acceptor.

CONCLUSIONS

There is a steady weakening progression in T-T bond strength as the tetrel atom grows larger. Whether neutral or positively or negatively charged, C_2Cl_4 contains a rather short and strong C=C double bond. But this bond strength fades quickly for the larger T atoms in the series, particularly for the neutral T_2Cl_4 species, where the T-T bond vanishes entirely for T larger than Ge. The $T_2Cl_4^-$ anions are more strongly bonded than the corresponding cations, which are in turn stronger than the neutrals. The bond appears to smoothly transition from covalent to a noncovalent bond. While this interaction might be referred to as a ditetrel bond, its origins are quite different in some ways than a conventional tetrel bond between an electron-deficient tetrel atom and an electron donor. This behavior differs from the simple T-T single bonds in the T_2H_6 and T_2Cl_6 molecules where the bond weakens much more slowly for larger T.

Acknowledgements

This material is based upon work supported by the National Science Foundation under Grant No. 1954310.

Conflict of Interest

The author declares no conflict of interest.

REFERENCES

1. D. E. Goldberg, D. H. Harris, M. F. Lappert and K. M. Thomas, *Chem. Commun.*, 1976, 261-262.
2. R. C. Fischer and P. P. Power, *Chem. Rev.*, 2010, **110**, 3877-3923.

3. E. Rivard and P. P. Power, *Inorg. Chem.*, 2007, **46**, 10047-10064.
4. T. Sugahara, J.-D. Guo, D. Hashizume, T. Sasamori and N. Tokitoh, *J. Am. Chem. Soc.*, 2019, **141**, 2263-2267.
5. M. Ma, L. Shen, H. Wang, Y. Zhao, B. Wu and X.-J. Yang, *Organometallics*, 2020, **39**, 1440-1447.
6. S. P. Green, C. Jones, P. C. Junk, K.-A. Lippert and A. Stasch, *Chem. Commun.*, 2006, 3978-3980.
7. J. Li, C. Schenk, C. Goedecke, G. Frenking and C. Jones, *J. Am. Chem. Soc.*, 2011, **133**, 18622-18625.
8. X. Wang, J. Liu, J. Yu, L. Hou, W. Sun, Y. Wang, S. Chen, A. Li and W. Wang, *Inorg. Chem.*, 2018, **57**, 2969-2972.
9. K. Chan, F. Ying, D. He, L. Yang, Y. Zhao, J. Xie, J.-H. Su, B. Wu and X.-J. Yang, *J. Am. Chem. Soc.*, 2024, **146**, 2333-2338.
10. Y. Zhao and D. G. Truhlar, *Theor. Chem. Acc.*, 2008, **120**, 215-241.
11. B. S. D. R. Vamhindi and A. Karton, *Chem. Phys.*, 2017, **493**, 12-19.
12. R. Podeszwa and K. Szalewicz, *J. Chem. Phys.*, 2012, **136**, 161102.
13. S. Karthikeyan, V. Ramanathan and B. K. Mishra, *J. Phys. Chem. A*, 2013, **117**, 6687-6694.
14. M. Majumder, B. K. Mishra and N. Sathyamurthy, *Chem. Phys.*, 2013, **557**, 59-65.
15. M. A. Vincent and I. H. Hillier, *Phys. Chem. Chem. Phys.*, 2011, **13**, 4388-4392.
16. A. D. Boese, *ChemPhysChem.*, 2015, **16**, 978-985.
17. M. Walker, A. J. A. Harvey, A. Sen and C. E. H. Dessent, *J. Phys. Chem. A*, 2013, **117**, 12590-12600.
18. L. F. Molnar, X. He, B. Wang and K. M. Merz, *J. Chem. Phys.*, 2009, **131**, 065102.
19. M. J. Frisch, G. W. Trucks, H. B. Schlegel, G. E. Scuseria, M. A. Robb, J. R. Cheeseman, G. Scalmani, V. Barone, G. A. Petersson, H. Nakatsuji, X. Li, M. Caricato, A. V. Marenich, J. Bloino, B. G. Janesko, R. Gomperts, B. Mennucci, H. P. Hratchian, J. V. Ortiz, A. F. Izmaylov, J. L. Sonnenberg, D. Williams-Young, F. Ding, F. Lipparini, F. Egidi, J. Goings, B. Peng, A. Petrone, T. Henderson, D. Ranasinghe, V. G. Zakrzewski, J. Gao, N. Rega, G. Zheng, W. Liang, M. Hada, M. Ehara, K. Toyota, R. Fukuda, J. Hasegawa, M. Ishida, T. Nakajima, Y. Honda, O. Kitao, H. Nakai, T. Vreven, K. Throssell, J. A. Montgomery Jr., J. E. Peralta, F. Ogliaro, M. J. Bearpark, J. J. Heyd, E. N. Brothers, K. N. Kudin, V. N. Staroverov, T. A. Keith, R. Kobayashi, J. Normand, K. Raghavachari, A. P. Rendell, J. C. Burant, S. S. Iyengar, J. Tomasi, M. Cossi, J. M. Millam, M. Klene, C. Adamo, R. Cammi, J. W. Ochterski, R. L. Martin, K. Morokuma, O. Farkas, J. B. Foresman and D. J. Fox, Wallingford, CT2016.
20. R. F. W. Bader, *Atoms in Molecules, A Quantum Theory*, Clarendon Press, Oxford, 1990.
21. T. A. Keith, TK Gristmill Software, Overland Park KS2013.
22. S. F. Boys and F. Bernardi, *Mol. Phys.*, 1970, **19**, 553-566.
23. K. Szalewicz and B. Jeziorski, in *Molecular Interactions. From Van der Waals to Strongly Bound Complexes*, ed. S. Scheiner, Wiley, New York1997, pp. 3-43.
24. R. Moszynski, P. E. S. Wormer, B. Jeziorski and A. van der Avoird, *J. Chem. Phys.*, 1995, **103**, 8058-8074.
25. D. G. A. Smith, L. A. Burns, A. C. Simmonett, R. M. Parrish, M. C. Schieber, R. Galvelis, P. Kraus, H. Kruse, R. D. Remigio, A. Alenaizan, A. M. James, S. Lehtola, J. P. Misiewicz, M. Scheurer, R. A. Shaw, J. B. Schriber, Y. Xie, Z. L. Glick, D. A. Sirianni,

J. S. O'Brien, J. M. Waldrop, A. Kumar, E. G. Hohenstein, B. P. Pritchard, B. R. Brooks, H. F. SchaeferIII, A. Y. Sokolov, K. Patkowski, A. E. DePrinceIII, U. Bozkaya, R. A. King, F. A. Evangelista, J. M. Turney, T. D. Crawford and C. D. Sherrill, *J. Chem. Phys.*, 2020, **152**, 184108.

26. P. Politzer and D. G. Truhlar, eds., *Chemical Applications of Atomic and Molecular Electrostatic Potentials*, Plenum, New York, 1981.
27. P. Politzer, P. Lane, M. C. Concha, Y. Ma and J. S. Murray, *J. Mol. Model.*, 2007, **13**, 305-311.
28. S. J. Grabowski, *Sci*, 2022, **4**, 17.
29. S. J. Grabowski, *Molecules*, 2020, **25**, 2703.
30. Y. N. Toikka, G. L. Starova, V. V. Suslonov, R. M. Gomila, A. Frontera, V. Y. Kukushkin and N. A. Bokach, *Cryst. Growth Des.*, 2023, **23**, 5194-5203.
31. R. M. Gomila, E. R. T. Tiekink and A. Frontera, *Inorganics*, 2023, **11**, 468.
32. C. Martín-Fernández, I. Alkorta, M. M. Montero-Campillo and J. Elguero, *ChemPhysChem.*, 2022, **23**, e202200088.
33. J. E. Del Bene, I. Alkorta and J. Elguero, *Phys. Chem. Chem. Phys.*, 2020, **22**, 15966-15975.
34. B. Eftekhari-Sis, I. García-Santos, A. Castiñeiras, G. Mahmoudi, E. Zangrando, A. Frontera and D. A. Safin, *CrystEngComm*, 2024, **26**, 1637-1646.
35. L. M. Azofra and S. Scheiner, *J. Chem. Phys.*, 2015, **142**, 034307.
36. N. Liu, X. Xie, Q. Li and S. Scheiner, *ChemPhysChem.*, 2021, **22**, 2305-2312.
37. J. J. Roeleveld, S. J. Lekanne Deprez, A. Verhoofstad, A. Frontera, J. I. van der Vlugt and T. J. Mooibroek, *Chem. Eur. J.*, 2020, **26**, 10126-10132.
38. S. Scheiner, *J. Phys. Chem. A*, 2021, **125**, 308-316.
39. S. J. Grabowski, *Phys. Chem. Chem. Phys.*, 2014, **16**, 1824-1834.
40. W. Zierkiewicz, M. Michalczyk, G. Mahmoudi, I. García-Santos, A. Castiñeiras, E. Zangrando and S. Scheiner, *ChemPhysChem.*, 2022, **23**, e202200306.
41. I. Alkorta and A. Legon, *Molecules*, 2018, **23**, 2250.
42. P. R. Varadwaj, A. Varadwaj, H. M. Marques and K. Yamashita, *CrystEngComm*, 2023, **25**, 1411-1423.
43. M. d. l. N. Piña, A. K. Sahu, A. Frontera, H. S. Biswal and A. Bauzá, *Phys. Chem. Chem. Phys.*, 2023, **25**, 12409-12419.
44. X. Wang, Q. Li and S. Scheiner, *Phys. Chem. Chem. Phys.*, 2023, **25**, 29738-29746.
45. L. Brammer, A. Peuronen and T. M. Roseveare, *Acta Cryst. C.*, 2023, **79**, 204-216.
46. S. A. Southern, T. Nag, V. Kumar, M. Triglav, K. Levin and D. L. Bryce, *J. Phys. Chem. C*, 2022, **126**, 851-865.
47. S. Liyanage, J. S. Ovens, S. Scheiner and D. L. Bryce, *Chem. Commun.*, 2023, **59**, 9001-9004.
48. K. Mandal, S. Sarkar, P. Ghosh, V. R. Hathwar and D. Chopra, *Acta Cryst. C.*, 2022, **78**, 597-605.
49. A. Grabarz, M. Michalczyk, W. Zierkiewicz and S. Scheiner, *ChemPhysChem.*, 2020, **21**, 1934-1944.
50. S. J. Grabowski, *Cryst.*, 2017, **7**, 43.
51. S. Scheiner, *J. Phys. Chem. A*, 2021, **125**, 2631-2641.
52. S. Scheiner, *Phys. Chem. Chem. Phys.*, 2020, **22**, 16606-16614.
53. H. Lin, L. Meng, X. Li, Y. Zeng and X. Zhang, *New J. Chem.*, 2019, **43**, 15596-15604.

54. K. J. Donald and M. Tawfik, *J. Phys. Chem. A*, 2013, **117**, 14176-14183.
55. Q. Tang and Q. Li, *Comput. Theor. Chem.*, 2014, **1050**, 51-57.
56. M. Marín-Luna, I. Alkorta and J. Elguero, *J. Organomet. Chem.*, 2015, **794**, 206-215.
57. M. Liu, Q. Li, W. Li and J. Cheng, *Struct. Chem.*, 2017, **28**, 823-831.
58. Y.-X. Wei, H.-B. Li, J.-B. Cheng, W.-Z. Li and Q.-Z. Li, *Int. J. Quantum Chem.*, 2017, **117**, e25448.
59. S. Scheiner, *J. Phys. Chem. A*, 2017, **121**, 5561-5568.
60. S. Scheiner, *Phys. Chem. Chem. Phys.*, 2021, **23**, 5702-5717.
61. Z. Wang, J. Zhang, J. Li and C. Cui, *J. Am. Chem. Soc.*, 2016, **138**, 10421-10424.

Table 1. Angle (degs) between T-T bond and TCl_2 planes in T_2Cl_4

T	$T_2Cl_4^-$	$T_2Cl_4^+$		Neut
	θ	θ_1	θ_2	θ
C	135.1	179.9	179.9	180.0
Si	105.5	149.1	149.1	123.4
Ge	103.0	141.0	141.0	118.9
Sn	100.5	110.8	173.6	-
Pb	91.0	109.6	165.8	-

Table 2. Dissociation energies (kcal/mol)

	T_2H_6	T_2Cl_6	$T_2Cl_4^-$	$T_2Cl_4^+$	T_2Cl_4
C	98.1	69.4	89.5 (89.3)[a]	120.0	121.1
Si	74.9	72.9	47.4 (47.3)	46.8	11.2
Ge	65.5	55.8	43.6 (41.9)	30.5	4.0
Sn	51.8	39.3	39.0 (38.1)	19.2	-
Pb	38.0	10.9	37.9 (37.0)	0.6	-

[a]values in parentheses computed with def2-QZVPP basis set

Table 3. AIM bond critical point densities (au) and Wiberg bond indices

	ρ					WBI				
T	T_2H_6,	T_2Cl_6	$T_2Cl_4^-$	$T_2Cl_4^+$	T_2Cl_4	T_2H_6,	T_2Cl_6	$T_2Cl_4^-$	$T_2Cl_4^+$	T_2Cl_4
C	0.2432	0.2350	0.2930	0.3043	0.3798	1.046	0.893	1.274	1.212	1.694
Si	0.0957	0.1051	0.0729	0.0946	0.0714	0.984	0.829	0.750	0.922	1.069
Ge	0.0842	0.0890	0.0569	0.0687	0.0398	0.975	0.803	0.629	0.723	0.597
Sn	0.0606	0.0618	0.0384	0.0378	-	0.935	0.761	0.506	0.492	-
Pb	0.0587	0.0528	0.0277	0.0207	-	0.873	0.605	0.337	0.231	-

Table 4. AIM total electron densities H and density Laplacian (au) at T--T bond critical point

	H					$\nabla^2\rho$				
T	T_2H_6	T_2Cl_6	$T_2Cl_4^-$	$T_2Cl_4^+$	T_2Cl_4	T_2H_6	T_2Cl_6	$T_2Cl_4^-$	$T_2Cl_4^+$	T_2Cl_4
C	-0.2064	-0.1854	-0.2909	-0.3093	-0.4076	-0.5941	-0.5467	-0.7882	-0.7689	-1.0338
Si	-0.0491	-0.0567	-0.0305	-0.0497	-0.0302	-0.1710	-0.2042	-0.0855	-0.1543	-0.0734
Ge	-0.0397	-0.0433	-0.0197	-0.0277	-0.0095	-0.0963	-0.1179	-0.0330	-0.0535	+0.0038
Sn	-0.0203	-0.0212	-0.0093	-0.0082	-	-0.0296	-0.0377	-0.0065	+0.0045	-
Pb	-0.0167	-0.0138	-0.0043	-0.0013	-	+0.0209	+0.0185	+0.0188	+0.0235	-

Table 5. SAPT partitioning of the total interaction energy into individual components (kcal/mol)

	ES	EX	IND	DISP	TOT
$Sn_2Cl_4^-$	-44.21	56.90	-48.08	-16.51	-51.90
$Sn_2Cl_4^+$(1)	-4.24	37.04	-52.21	-11.05	-30.46
$Sn_2Cl_4^+$(2)	10.52	32.17	-61.81	-9.97	-29.09
$Pb_2Cl_4^-$	-37.76	44.41	-37.36	-16.32	-47.03
$Pb_2Cl_4^+$(1)	13.81	13.89	-23.87	-7.03	-3.20
$Pb_2Cl_4^+$(2)	19.36	11.16	-28.64	-6.45	-4.57

(1) places charge on upper unit, (2) on lower unit

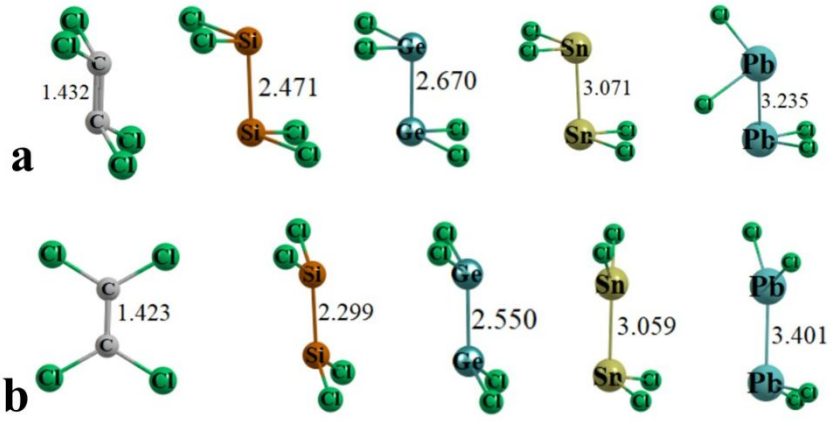

Fig 1. Optimized geometries of a) $T_2Cl_4^-$ and b) $T_2Cl_4^+$. Distances in Å.

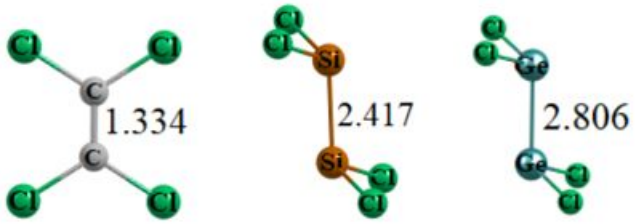

Fig 2. Optimized geometries of neutral T_2Cl_4. Distances in Å.

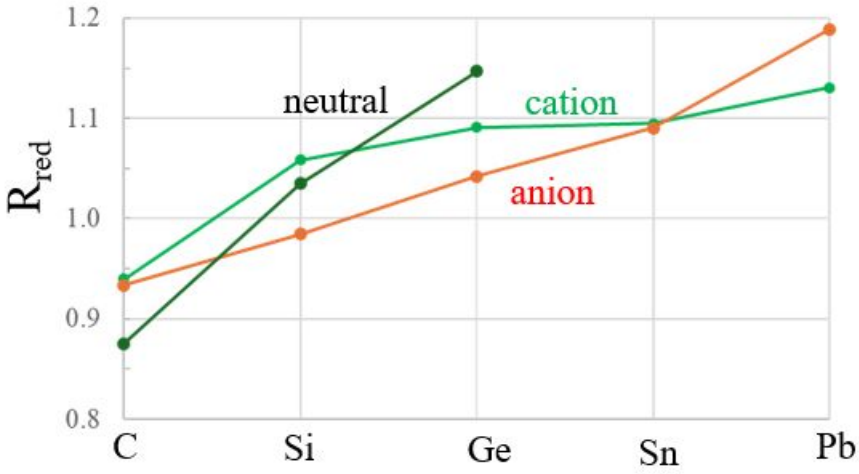

Fig 3. Reduced T-T bondlengths for T_2Cl_4 systems.

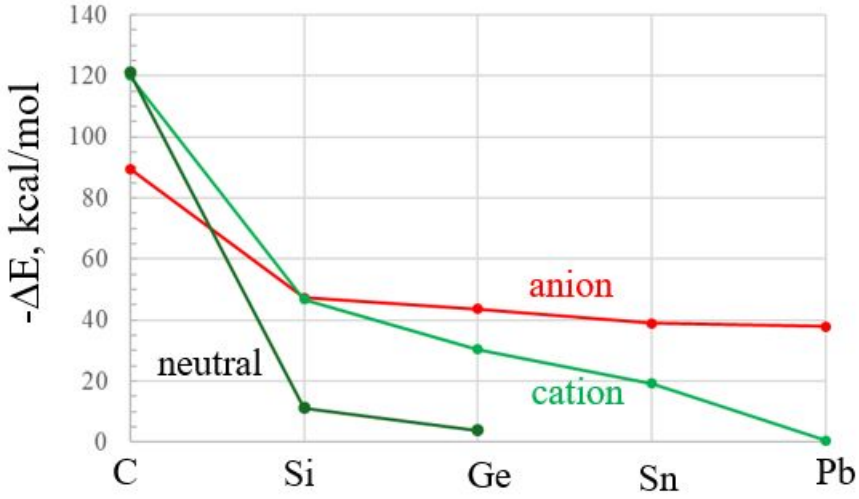

Fig 4. Association energies of T_2Cl_4 systems.

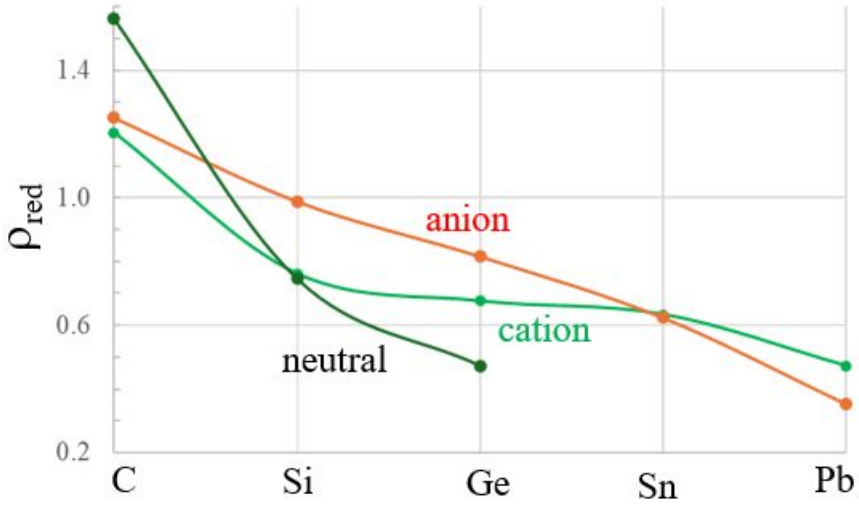

Fig 5. T-T bond critical point densities of T_2Cl_4 systems, reduced by division by the same quantity in T_2H_6.

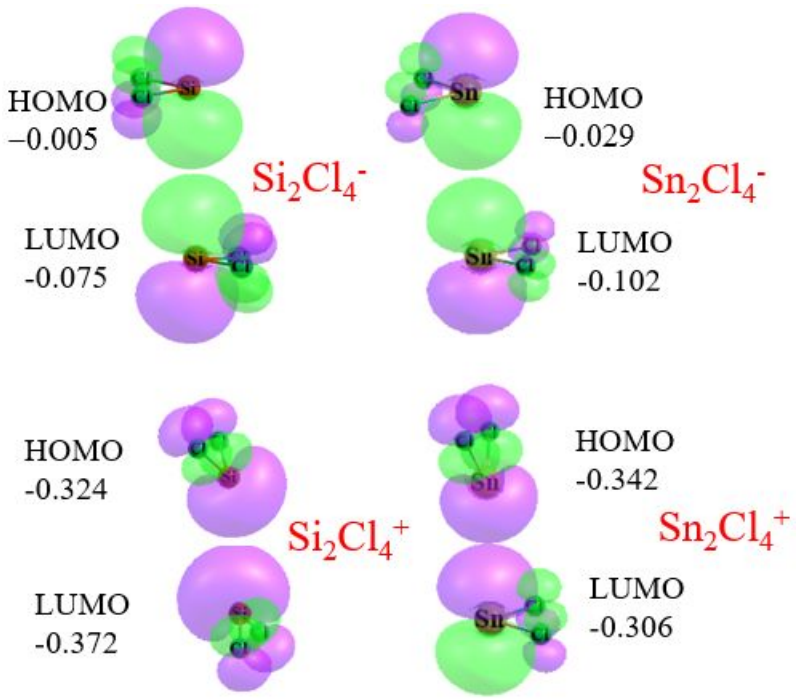

Fig 6. Alignment of HOMO and LUMO of monomers within the context of the indicated T_2Cl_4 systems. Purple and green colors indicate opposite sign of the wavefunction. Orbital energies in au.

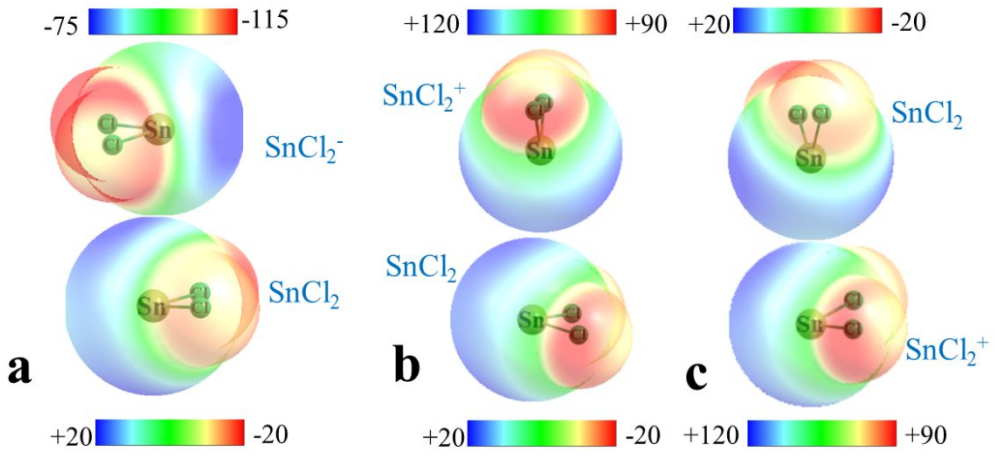

Fig 7. Molecular electrostatic potentials (kcal/mol) of monomers, and their alignment within a) $Sn_2Cl_4^-$ and $Sn_2Cl_4^+$, with cationic charge assigned to b) upper and c) lower unit.

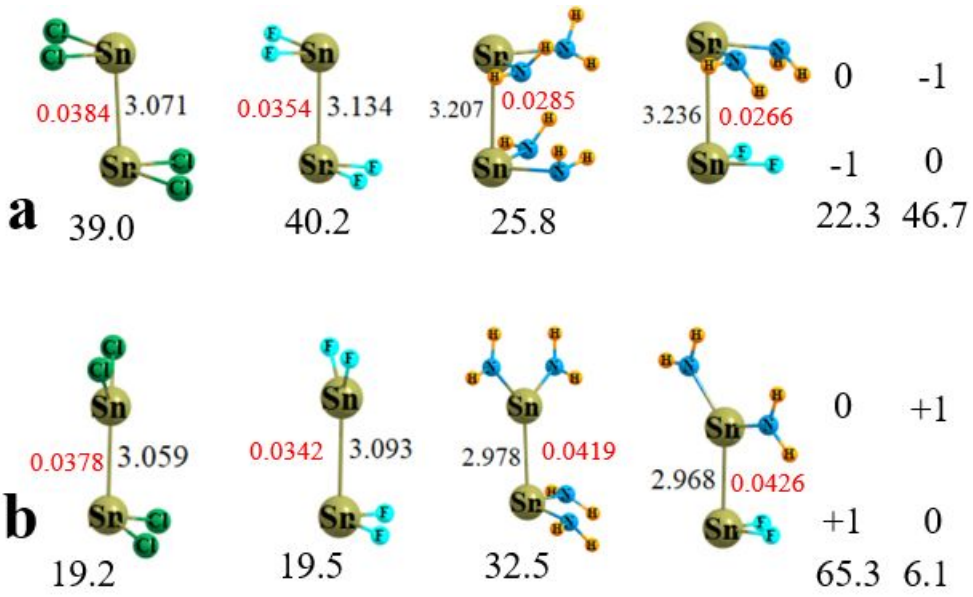

Fig 8. Optimized geometries of a) anions and b) cations of indicated systems. Distances in Å, BCP densities (au) in red, and association energies (kcal/mol) in black. The dissociation energies of the mixed system are indicated for each of the two possible assignments of charge on upper and lower units.

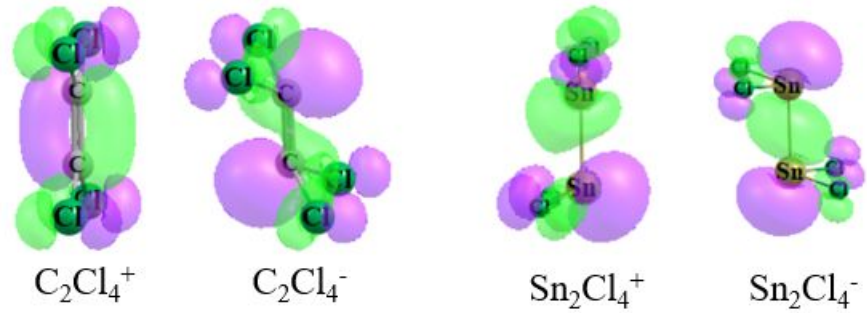

Fig 9. Singly occupied molecular orbital of indicated ions. Purple and green colors indicate opposite sign of the wavefunction.